Sensors and Materials, Vol. 30, No. 11 (2018) 2391–2400
MYU Tokyo

S & M 1684

Numerical Study of Thermal Performance of Phase Change Material-based Heat Sinks with Three-dimensional Transient Cooling

Ju-Ho Jeong,[1] Jin Hyun Lee,[2*] and Sung-Min Kim[1**]

[1]School of Mechanical Engineering, Sungkyunkwan University,
300 Cheoncheon-dong, Suwon 16419, Republic of Korea
[2]Polymer Technology Institute, Sungkyunkwan University,
300 Cheoncheon-dong, Suwon 16419, Republic of Korea

(Received January 18, 2018; accepted June 19, 2018)

Keywords: phase change material (PCM), paraffin wax, heat sink, melting

A three-dimensional numerical model is constructed to examine the thermal performance of a phase change material (PCM)-based heat sink. The PCM is stored in a rectangular heat sink and a uniform heat flux is applied at the bottom of the heat sink. The PCM used in this model is paraffin wax and the heat sink is made of aluminum. Numerical transient simulations are conducted with different power levels (15, 20, and 25 W). As the power level increases, the melting rate increases and the melting time decreases. The convection of liquid PCM is observed by monitoring the temperature and velocity vector inside the PCM. During the melting process, the convection effect is enhanced by increasing the amount of molten PCM.

1. Introduction

The ability to dissipate large amounts of heat from small surface areas is important in designing many advanced electronic devices because effective thermal management is essential in maintaining the performance of these devices. A phase change material (PCM)-based cooling system that utilizes passive cooling can dissipate heat effectively using phase change (i.e., latent heat of PCM) with a small volume change during melting and solidification. A key challenge in designing cooling systems using PCM is to enhance the low thermal conductivity of PCM. The heat transfer performance can be improved by using the heat sink owing to the high thermal conductivity of internal metal fins.

The thermal performance of PCM-based heat sinks for various design parameters was numerically investigated. A numerical model was constructed to simulate the melting and solidification of PCM by Shatikian *et al.*[(1)] Also, the effects of various fin heights and thicknesses of PCM-based heat sinks were investigated for constant temperature and heat flux conditions.[(2,3)] The dimensional analysis of the results shows that the melt fraction and Nusselt number depend on the combination of the Fourier, modified Stefan and Rayleigh numbers. Wang *et al.* numerically studied the effects of the orientation of the heat sinks on the

*Corresponding author: e-mail: alee@skku.edu
**Corresponding author: e-mail: smkim@skku.edu
https://doi.org/10.18494/SAM.2018.1974

ISSN 0914-4935 © MYU K.K.

thermal performance of the cooling system.[4] The computed results show that the time to melt completely is delayed by increasing the degree of tilting of the heat sink. Several additional parameters such as the amount of PCM and the aspect ratio of the heat sink and different PCMs were examined. As the amount of PCM or the aspect ratio of the heat sink increases, the time to reach the maximum temperature of the PCM is delayed.[5] Wang and Yang investigated the influence of the number of fins on the melting of the PCM under both heating and nonheating conditions. The temperature gradient of the system is kept stable as the number of fins of the PCM-based heat sink increases.[6] Pakrouh *et al.* optimized the geometrical parameters of the PCM-based pin-fin heat sink, such as the number of fins, the fin height, the fin thickness, and the base thickness for different critical temperatures.[7] Ji *et al.* numerically investigated a rectangular thermal energy storage system with PCM heated vertically from one side. To improve the nonuniform heat transfer to the PCM, two fins with different inclined angles attached to the heating surface are used.[8]

The thermal performance of the PCM-based heat sink was also studied experimentally. In the study of Kandasamy *et al.*, with increasing power level in the melting process, the melting rate of the PCM and the cooling performance of the PCM-based heat sink increase.[9] Hosseinizadeh *et al.* investigated the effect of the number of fins of the heat sink. The case temperature of the heat sink during the melting process decreases with increasing number, height, and thickness of fins.[10] In the study of Gharbi *et al.*, the thermal performance of three different PCMs (a plastic paraffin PCM and two composite PCMs of PCM/silicone matrix and PCM/graphite matrix) was examined experimentally. The result reveals that the graphite matrix filled with PCM shows the best performance. They also confirmed that PCM-based heat sinks having internal fins improve the heat distribution in the PCM.[11] Srikanth and Balaji performed experiments to investigate the thermal performance of PCM-based cuboidal heat sinks with 72 pin-fins.[12] Heat transfer correlations were developed for the characteristic time for phase change with natural convection as a function of the individual power levels. Arshad *et al.* examined the thermal performance of PCM-based pin-fin heat sinks having different pin-fin thicknesses of 1, 2, and 3 mm. When the amounts of PCM filled in the heat sink are 33 and 66%, the thermal performance of the heat sink with a 3 mm pin-fin is higher than that with a 2 mm pin-fin.[13] The thermal performance of pin-finned heat sinks with a round pin-fin was examined by Arshad *et al.* to explore the effects of pin-fin diameter, input heat flux, and volumetric fraction of PCM. The results show that the heat sink with a 3 mm pin diameter shows the best thermal performance.[14]

In this study, a three-dimensional numerical model of a PCM-based heat sink was developed to assess the thermal performance of the heat sink. Numerical studies were conducted with different power levels (15, 20, and 25 W) from the bottom surface of the heat sink.

Nomenclature

A, B	Constants in Eq. (2)
A_{mush}	Mushy zone constant
c_p	Specific heat
G	Gravitational acceleration
H	Latent heat

H	Enthalpy
I	Unit tensor
k_f	Liquid thermal conductivity
ks	Solid thermal conductivity
q	Power level
q''	Heat flux
S	Momentum source
T	Temperature
T_m	Melting temperature
t	Time
u	Velocity
x, y, z	Spatial coordinates

Greek symbols

β	Volumetric coefficient of expansion
ε	Small number
μ	Dynamic viscosity
ρ	Density
ρ_m	Density of PCM at melting temperature
φ	Liquid fraction

Subscripts

n	Phase of fluid
s	Solid

2. Numerical Model

2.1 Physical model

A schematic of a three-dimensional physical model of a PCM-based heat sink is shown in Fig. 1. Taking advantage of symmetry, the computational domain is composed of a unit cell of a heat sink. Figure 2 shows an orthographic view of the unit cell with detailed dimensions. The cavity of the heat sink is filled with PCM. Because of the expansion of the PCM, the amount of the PCM is only 90% of the cavity volume (i.e., the height of the PCM is 14.4 mm) and the remaining 10% of the cavity volume is filled with air. To incorporate the effect of the natural convection of the PCM, the gravitational acceleration of 9.81 m/s^2 is considered in the negative

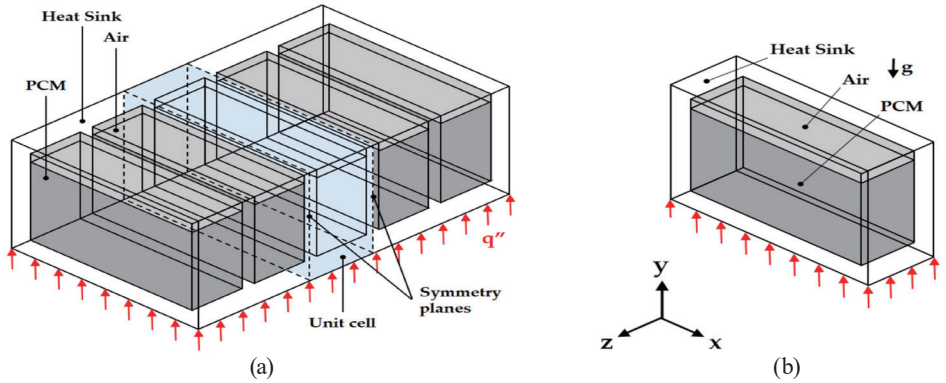

Fig. 1. (Color online) Three-dimensional (a) physical model and (b) unit cell of PCM-based heat sink.

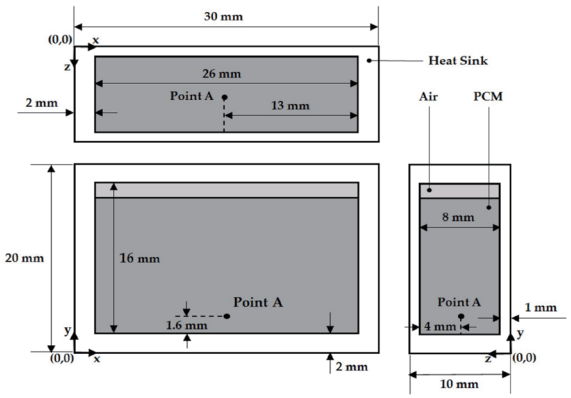

Fig. 2. Orthographic view of unit cell of PCM-based heat sink.

y-direction. The uniform heat flux is applied at the bottom surface (y = 0 mm) of the heat sink, while the top (y = 20 mm) and side (z = 0, 10 mm) surfaces of the heat sink are assumed adiabatic and symmetric, respectively, as illustrated in Fig. 1(a).

2.2 Materials

Paraffin wax is used as the PCM and the heat sink is made of aluminum. The thermophysical properties of the paraffin wax are obtained from Ref. 4, and detailed property values for all materials used in the present study are summarized in Table 1.[4]

The density of air depends on its temperature, and the density of the PCM can be expressed as

$$\rho = \rho_m/[\beta(T - T_m) + 1], \tag{1}$$

where ρ_m is the density of the PCM at the melting temperature.[2] The volumetric coefficient of expansion of $\beta = 0.001$ K^{-1} is chosen on the basis of the data reported by Humphries and Griggs.[15] The thermal conductivity of the solid PCM is k_s when $T < T_m$, while that of the liquid PCM is k_f when $T > T_m$. The PCM starts to melt at the solidus temperature T_{sol} of 46 °C and the PCM melting process is complete at the liquidus temperature T_{liq} of 48 °C. The dynamic viscosity of the liquid PCM can be expressed as

$$\mu = e^{A+B/T}, \tag{2}$$

where $A = -4.25$ and $B = 1790$.[2,16]

2.3 Numerical methods

Three-dimensional numerical simulations are carried out using the FLUENT 16.2 computational fluid dynamics (CFD) code with the Pressure Implicit with Splitting of Operator (PISO) scheme and the Volume of Fluid (VOF) model in the Multiphase Model.[17,18] The

Table 1
Thermophysical properties of paraffin wax, aluminum, and air.[4]

Material	ρ (kg/m^3)	c_p (J/kgK)	k_f (W/mK)	k_s (W/mK)	T_m (°C)	ΔH (J/kg)
Paraffin wax	$750/[0.001(T-319.15)+1]$	2890	0.12	0.21	46–48	173400
Aluminum	2719	8741	—	202.4	—	—
Air	$1.2\times10^{-5}T^2-0.01134T+3.498$	1006.4	0.0242	—	—	—

courant number between 0.1 and 1.0 is used to obtain a converged solution in each case. The method of meshing is quadrilateral dominant with a uniform element size of 0.001 m. The grid independence test is performed by monitoring the PCM liquid fraction for different numbers of cells (21463, 33511, 48591, and 63289 cells). The difference in melting time between 48591 and 63289 cells is 0.64%; therefore, the grid system with 48591 cells is chosen.

The three-dimensional temperature distribution in the solid aluminum is obtained by solving the energy conservation equation.[17]

$$\frac{\partial}{\partial t}(\rho_s h) = \nabla\cdot(k_s \nabla T) \tag{3}$$

In the present numerical model, two types of fluid are defined as follows.

Primary phase (n = 1): air
Secondary phase (n = 2): paraffin wax

For both phases, the mass conservation, momentum conservation, and energy conservation can be respectively expressed as[17]

$$\frac{\partial}{\partial t}(\rho_n) + \nabla\cdot(\rho_n \vec{u}) = 0, \tag{4}$$

$$\frac{\partial}{\partial t}(\rho_n \vec{u}) + \nabla\cdot(\rho_n \vec{u}\vec{u}) = -\nabla p + \nabla\cdot[\mu_n(\nabla\vec{u} + \nabla\vec{u}^{\mathrm{T}} - \frac{2}{3}\nabla\cdot\vec{u}I)] + \rho_n\vec{g} + \vec{S}_n, \tag{5}$$

$$\frac{\partial}{\partial t}(\rho_n h) + \nabla\cdot(\rho_n \vec{u} h) = \nabla\cdot(k_n \nabla T). \tag{6}$$

In the momentum conservation equation, the momentum source for air is $\vec{S}_1 = 0$ because there is no melting process. The momentum source for the PCM, $\vec{S}_2$, can be expressed as

$$\vec{S}_2 = -A(\varphi)\vec{u}, \tag{7}$$

where $A(\varphi)$, the porosity function defined by Brent *et al.*,[19] can be written as

$$A(\varphi) = A_{mush} \frac{(1-\varphi)^2}{\varphi^3 + \varepsilon}, \tag{8}$$

with $A_{mush} = 10^5$ and $\varepsilon = 0.001$ in this study. ε should be small to avoid division by zero and A_{mush} is a mushy zone constant that measures the damping amplitude of the PCM.

3. Results

3.1 Variation in temperature with time

The average temperatures of the bottom surface of the heat sink with and without the PCM are presented in Fig. 3(a). In the case of the heat sink without the PCM, the average temperature increases sharply. In the case of the heat sink with the PCM, until the PCM starts to melt, the average temperature of the bottom surface increases slowly relative to the heat sink without the PCM. This is because the specific heat of the PCM is higher than that of air. After the temperature of the PCM reaches its melting temperature, the temperature increases slowly owing to the melting of the PCM, and then starts to increase steeply when the PCM melts completely.

Figure 3(b) shows the temperature variation at Point A that is located inside the PCM. The local temperature bump between 200.8 and 290.7 s can be explained by Fig. 4. The temperature at Point A increases over time since the molten PCM moves upward through Point A owing to the natural convection inside the PCM [see Fig. 4(a)]. The effect of natural convection of the liquid PCM is increased by increasing the amount of molten PCM. After 250.6 s, the solid PCM that maintains the melting temperature moves toward the bottom of the cavity because its density is higher than that of the liquid PCM [see Figs. 4(a) and 4(b)]. Thus, the temperature at Point A decreases until the complete melting of the PCM at 290.7 s.

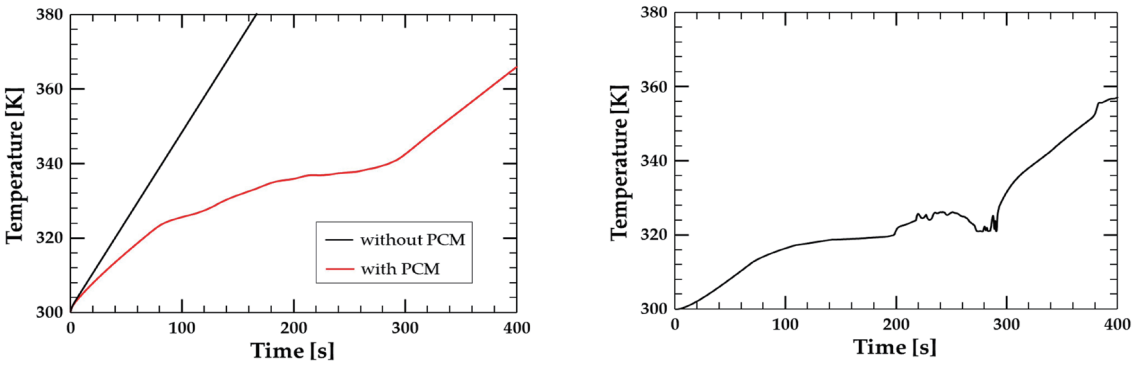

Fig. 3. (Color online) Variations in (a) average temperatures of the bottom surfaces of the heat sinks without and with PCM and (b) local temperature at Point A for q = 15 W.

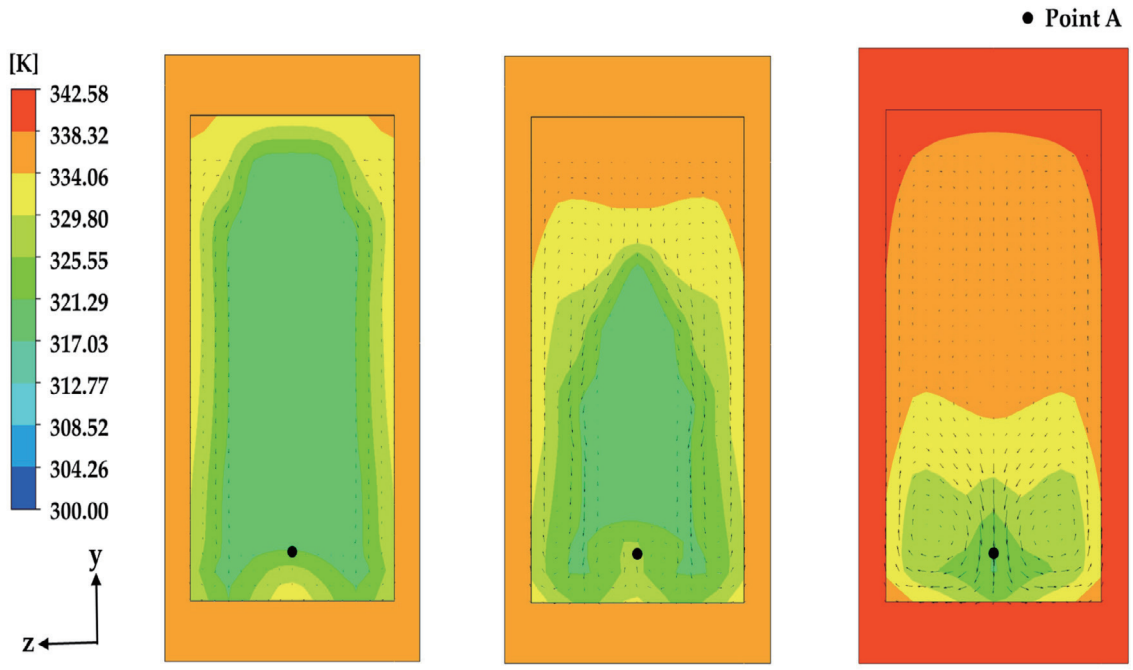

Fig. 4. (Color online) Temperature distribution and velocity vector of the PCM-based heat sink at the plane of x = 15 mm for q = 15 W: (a) t = 200.8 s, (b) t = 250.6 s, and (c) t = 290.7 s.

3.2 Effect of power level

Figure 5(a) shows PCM liquid fraction versus time for different power level q values of 15, 20, and 25 W, corresponding to the heat flux from the bottom surface of the heat sink, q'' = 1.00, 1.33, and 1.67 W/cm^2, respectively. The times to start the melting of the PCM are 64.9, 46.0, and 35.1 s, and the melting times of the PCM are 226.6, 185.1, and 158.9 s for q = 15, 20, and 25 W, respectively. As expected, the time to start the melting and the melting time decrease with increasing power level. As also shown in Fig. 5(a), the melting rate of the PCM, which is the slope of the PCM liquid fraction during the melting process, begins to decrease during the melting process, and the specific locations where the melting rate of the PCM changes are indicated in Fig. 5(a) using black circles for different power levels. The PCM starts to melt from the outside of the cavity. When the outside of the PCM melts completely, the region between the solid PCM and the heat sink surfaces becomes filled with molten PCM. Since the thermal conductivity of the liquid PCM is lower than that of the solid PCM, the effect of heat conduction is diminished, resulting in a lower melting rate.

Figure 5(b) shows the variations in average temperature at the bottom surface of the heat sink. Similar trends of temperature variations with time are observed in the q = 20 and 25 W cases, while showing a higher rate of temperature increase for a higher power level. As shown in Fig. 5(c), the local temperature bumps inside the PCM are also observed for higher power levels, which suggests that the natural convection of the liquid PCM plays an important role in the PCM-based heat sink.

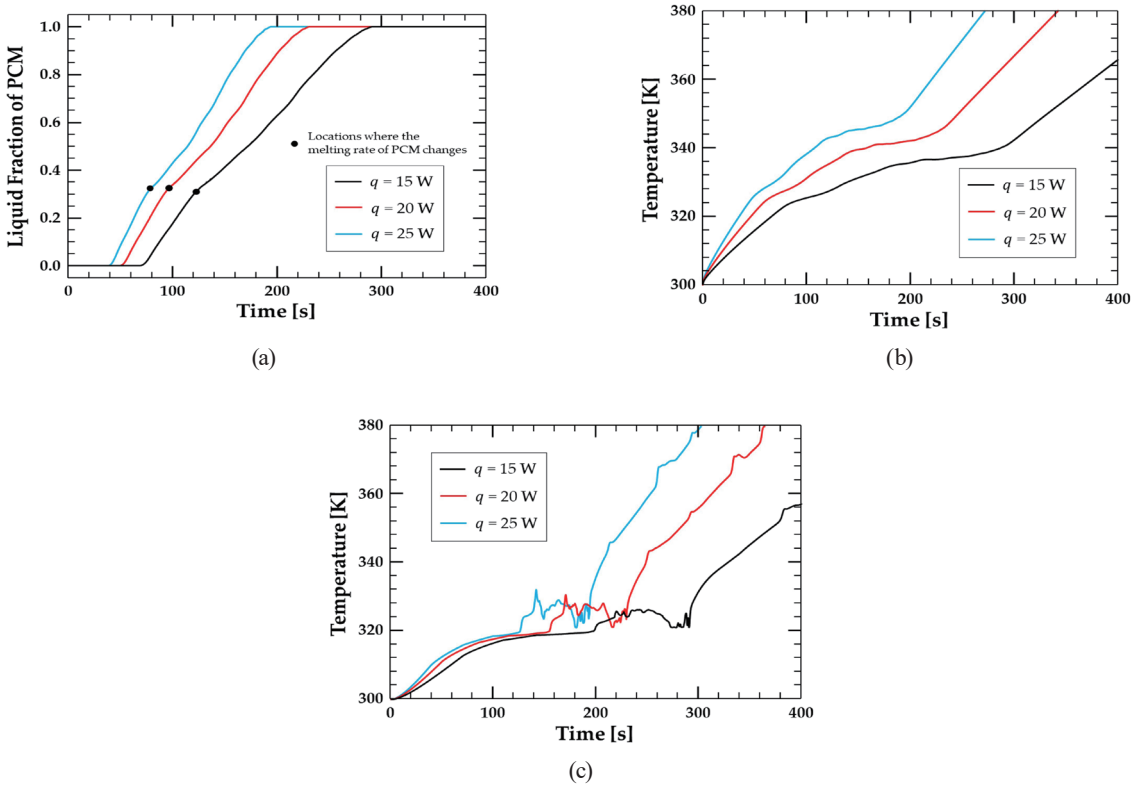

Fig. 5. (Color online) Variations in (a) liquid fraction of PCM, (b) average temperature at bottom surface of heat sink, and (c) local temperature at Point A for different power levels.

Figure 6 shows the temperature distribution of the PCM surface and the PCM liquid fraction for different power levels at around 100 s. Since the heat transfer occurs from the internal metal fins to the PCM, the outside of the PCM starts to melt first. Thus, the temperature of the outside of the PCM is higher than that of the inside. The temperature of the molten PCM continuously increases over time owing to its sensible heat increase, whereas the temperature of the solid PCM is maintained with the melting temperature. Therefore, in all three cases, the temperature of the top surface of the PCM where most of the PCM is solid is much lower than in other regions. In addition, with increasing power level, the region of the molten PCM between the solid PCM and the heat sink surface becomes thicker.

4. Conclusions

In this study, we explored the melting process of paraffin wax in a rectangular heat sink. A three-dimensional physical model was tested for different power levels by monitoring the average temperature of the bottom surface of the heat sink and the PCM liquid fraction. The key conclusions from this study can be summarized as follows:

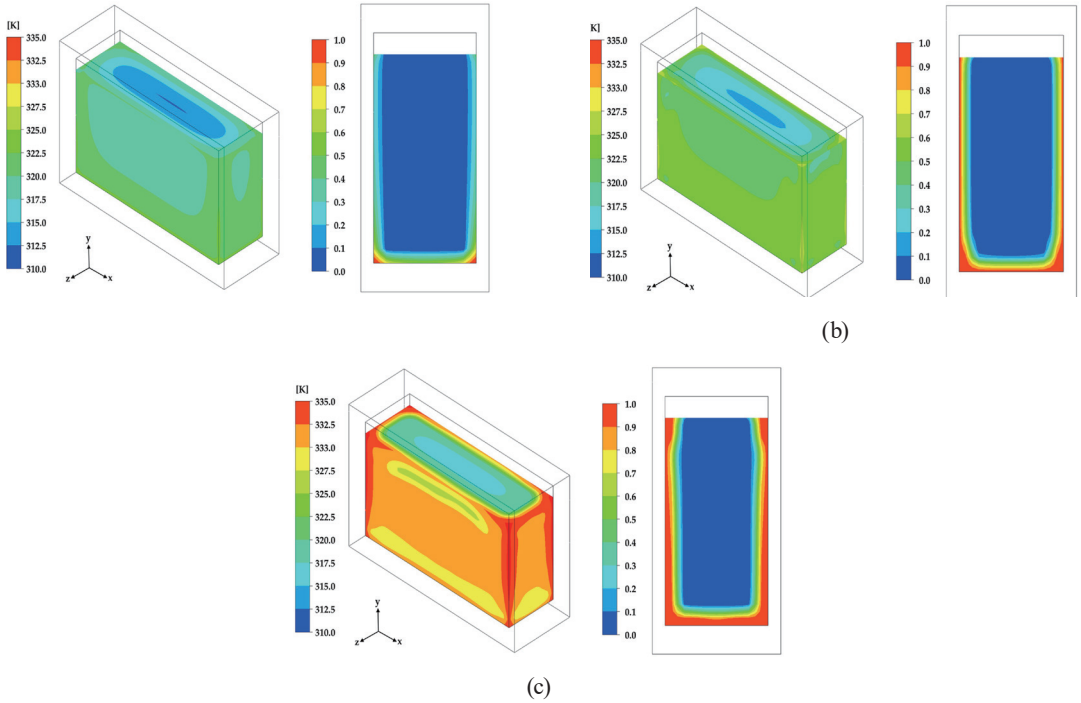

Fig. 6. (Color online) Temperature distribution of PCM surface and liquid fraction of PCM at plane of x = 15 mm for (a) q = 15 W, t = 100.3 s, (b) q = 20 W, t = 100.6 s, and (c) q = 25 W, t = 100.3 s.

(1) A three-dimensional numerical model is developed to simulate the phase change process in a PCM-based heat sink having rectangular cavities.
(2) The PCM-based heat sink enhances the cooling performance as compared with the heat sink without the PCM for the same heat flux.
(3) The convection effect of the liquid PCM is enhanced by increasing the amount of molten PCM during the melting process.
(4) As the power level increases, the PCM starts to melt earlier and the melting time decreases.
(5) The melting rate of the PCM begins to decrease during the melting process since the effect of heat conduction is diminished by the low thermal conductivity of the liquid PCM.

Acknowledgments

This work was supported by the National Research Foundation of Korea (NRF) grant funded by the Korea government (MSIP) (No. NRF-2015R1C1A1A01055439).

References

1 V. Shatikian, V. Dubovsky, G. Ziskind, and R. Letan: Proc. ASME 2003 Heat Transfer Summer Conference (ASME, Minneapolis, 2003) 347–353. https://doi.org/10.1115/ht2003-47167
2 V. Shatikian, G. Ziskind, and R. Letan: Int. J. Heat Mass Transfer **48** (2005) 3689. https://doi.org/10.1016/j.ijheatmasstransfer.2004.10.042

3 V. Shatikian, G. Ziskind, and R. Letan: Int. J. Heat Mass Transfer **51** (2008) 1488. https://doi.org/10.1016/j.ijheatmasstransfer.2007.11.036
4 X. Q. Wang, A. S. Mujumdar, and C. Yap: Int. Commun. Heat Mass Transfer **34** (2007) 801. https://doi.org/10.1016/j.icheatmasstransfer.2007.03.008
5 X. Q. Wang, C. Yap, and A. S. Mujumdar: Int. J. Therm. Sci. **47** (2008) 1055. https://doi.org/10.1016/j.ijthermalsci.2007.07.016
6 Y. H. Wang and Y. T. Yang: Energy. **36** (2011) 5214. https://doi.org/10.1016/j.energy.2011.06.023
7 R. Pakrouh, M. J. Hosseini, A. A. Ranjbar, and R. Bahrampoury: Energy Convers. Manage. **103** (2015) 542. https://doi.org/10.1016/j.enconman.2015.07.003
8 C. Ji, Z. Qin, Z. Low, S. Dubey, F. H. Choo, and F. Duan: Appl. Therm. Eng. **129** (2018) 269. https://doi.org/10.1016/j.applthermaleng.2017.10.030
9 R. Kandasamy, X. Q. Wang, and A. S. Mujumdar: Appl. Therm. Eng. **28** (2008) 1047. https://doi.org/10.1016/j.applthermaleng.2007.06.010
10 S. F. Hosseinizadeh, F. L. Tan, and S. M. Moosania: Appl. Therm. Eng. **31** (2011) 3827. https://doi.org/10.1016/j.applthermaleng.2011.07.031
11 S. Gharbi, S. Harmand, and S. B. Jabrallah: Appl. Therm. Eng. **87** (2015) 454. https://doi.org/10.1016/j.applthermaleng.2015.05.024
12 R. Srikanth and C. Balaji: INAE Lett. **2** (2017) 65. https://doi.org/10.1007/s41403-017-0024-x
13 A. Arshad, H. M. Ali, M. Ali, and S. Manzoor: Appl. Therm. Eng. **112** (2017) 143. https://doi.org/10.1016/j.applthermaleng.2016.10.090
14 A. Arshad, H. M. Ali, S. Khushnood, and M. Jabbal: Int. J. Heat Mass Transfer **117** (2018) 861. https://doi.org/10.1016/j.ijheatmasstransfer.2017.10.008
15 W. R. Humphries and E. I. Griggs: A Design Handbook for Phase Change Thermal Control and Energy Storage Devices (National Aeronautics and Space Administration, Huntsville, 1977).
16 R. C. Reid, J. M. Prausnitz, and T. K. Sherwood: The Properties of Gases and Liquids (McGraw Hill, New York, 1987) pp. 439–456.
17 Ansys. Inc.: ANSYS FLUENT 15.0 in Workbench User's Guide (2013).
18 C. W. Hirt and B. D. Nichols: J. Comput. Phys. **39** (1981) 201. https://doi.org/10.1016/0021-9991(81)90145-5
19 A. D. Brent, V. R. Voller, and K. T. J. Reid: Numer. Heat Transfer, Part A. **13** (1988) 297. https://doi.org/10.1080/10407798808551388